Response Analysis of Long Drilling Risers in Re- Entry to Horizontal Oscillation of Mother Vessels*

DAI Si-yu (代思宇), CHEN Wei (陈威), XU Xue-song (徐雪松)[1]

State Key Laboratory of Ocean Engineering, Shanghai Jiaotong University, Shanghai 200240, China

Abstract: In re-entry, the free-hanging riser will oscillate under horizontal oscillation of Mother Vessel (MV), which can cause the connection difficulty of the riser lower end with the seabed wellhead in re-entry. In this study, Flexible Segment Model (FSM) based dynamic calculation method is employed to predict riser response under horizontal oscillation of MV. Different oscillation periods and amplitudes of MV are selected as the motion input of the riser upper end. The numerical results of inline oscillation of a riser model are shown in the paper, which have a good match with the experimental results. The dynamic response of the lower end of a 1500-meter riser to the horizontal oscillation of MV is analyzed, and the Minimum- Oscillation Point (MOP) along the riser is located.

Key words: *numerical analysis; riser oscillation; freely-hanging marine riser; riser re-entry*

1. Introduction

With the accelerating pace of deep ocean oil and gas exploration, more significance is attached to the research on ocean platform and marine risers. Marine risers are vital connectors between MVs and the seabed wellhead. Oscillations of marine risers can be induced by two categories of excitations: vessel motions and hydrodynamic loads (Lucile et al., 2013). Plenty of researches focus on riser response excited by hydrodynamic loads, such as waves, ocean currents and vortices (Xu et al., 2009; Yang et al., 2012; Yang and Xiao, 2014; Dai et al., 2014; Chen et al.,

* This project was financially supported by the National Natural Science Foundation of China (Grant 51279107) and The National Science and Technology Major Project (Grant 2011ZX05027-004-05).

1 Corresponding author. E-mail: xsxu@sjtu.edu.cn

2014), whereas studies on riser oscillations induced by vessel motions are still inadequate (Xu and Wang, 2012; Bai et al, 2014; Wang et al, 2014). Actually, during riser re-entry, the mother vessel will experience horizontal oscillations induced by complex environmental forces. The free-hanging riser will oscillate under vessel motion, which introduces difficulty when connecting riser lower end with the seabed wellhead (Xu et al, 2013). In order to carry out a cost-effective installation, it is necessary to predict riser response under different motion input from mother vessel, since vessel motion is one of the major excitations of riser oscillation.

Dynamic calculation is prevalent in the current researches on prediction of riser response, of which there are two main categories of methods: consecutive method and discrete method. As for consecutive method, the governing equations of marine risers are often deduced from Hamilton's Principle and the role of model functions is to estimate the dynamic response of the whole riser rather than a particular segment (Hong, 2004; Do and Pan, 2008a, 2008b; Lucor and Triantafyllou, 2008). An instance of consecutive method is the systematic research on dynamic calculations of a flexible marine riser conducted by Hong Y. P. et al (2004). In this study, a series of complex differential and integral governing equations were deduced from Hamilton's Principle, and Galerkin Method was applied in order to obtain the approximate numerical solution of the equations. By virtue of the appropriate selection of model functions, which is a critical step of consecutive method, the results of dynamic calculation had relatively high accuracy.

With regard to the discrete method, researchers often divide the slender body into an appropriate quantity of segments (Park and Jung, 2002, 2003; Raman-nair and Baddour, 2003). Instead of taking the whole riser into account during the initial dynamics analysis, the discrete method base governing equations on force and moment equilibrium equations of each particular segment. Park et al. (2003) illustrated a discrete method of dynamic calculation, which was applied to towed low cables. An implicit finite difference algorithm and Newton-Rapson iteration scheme were employed respectively to deal with the three-dimensional equations of cable and the problem of hydrodynamic and geometric nonlinearities. Xu (2012)

proposed a Flexible Segment Model (FSM) for underwater slender bodies. In the FSM, a slender body was discretized into a series of flexible curved segments. The deformation of the whole slender body was decomposed into micro-deformations of all flexible segments. The governing equations were listed according to the moment equilibrium on these segments. FSM is employed in the present study to analyze riser dynamic response because of its ease of implement and reduced computation scale, while maintaining the convergence and accuracy.

This paper is further organized as follows: Section 2 will introduce the FSM and the dynamic calculation; Section 3 will show the validation of the FSM based dynamic calculation; Section 4 will demonstrate the dynamic response of the lower end of a 1500-meter riser in real ocean engineering, and locate the minimum-oscillation points (MOPs) along the riser. Section 5 will sum up the results of numerical analysis.

2. Physical Model and Numerical Calculation

2.1 Flexible Segment Model

In re-entry, the upper end of the marine riser is connected with the MV, while the lower end keeps a free state, without any connection with the seabed wellhead (Kajiwara and Noridomi, 2009). As discussed by Xu (2012), there are two typical types of connection method between the riser and the mother vessel, fixed connection and free connection. Different connection methods bring about different boundary conditions in dynamic analysis of riser. Usually, a bottom object，such as Christmas Tree or Blow-off Preventer, is also attached to the lower end of the marine riser, as shown in Fig.1 (a). The riser is assumed to oscillate in a 2D global coordinate system, in which X-axis is horizontal, pointing to the forwarding direction, while Y-axis is vertical, pointing to the sea bottom. Mother vessel needs to be moved along the X-axis for the purpose of repositioning the riser lower end to the target location right above the wellhead.

To make the dynamic calculation, FSM (Xu, 2012) is put to use. As shown in Fig.1(b), the riser is viewed as a slender cylinder, discretized into n flexible segments marked by $S_1, S_2, \ldots, S_n$. There are altogether $n+1$ nodes at the ends of all segments,

denoted by $N_1, N_2, \ldots, N_n, N_{n+1}$. To analyze the deformation of each segment, the magnified local area about S_i is illustrated in Fig.1(c).

The free-hanging riser in re-entry may take on lateral deflection and axial elongation, respectively caused by bending moment and axial tension. Considering that lateral deflection is the main part of riser deformation, here we focus on the lateral deflection caused by the bending moment, and the elongation by tension is neglected, as did by Xu (2012).

The bending moments at N_i and N_{i+1} are represented by m_i and m_{i+1}, and the bending moment is assumed to be distributed linearly along the riser, denoted by

$$m = m_i + (m_{i+1} - m_i)\frac{l}{l_i} \tag{1}$$

where l_i is the length of S_i, m is the bending moment of a point between N_i and N_{i+1}, l denotes the distance of the point from N_i.

2.1.1 Deflection Feature of Segments

To illuminate the deflection feature of segments, the following angles are denominated, as is shown in Fig.1(b):

Node Angle φ_i is the angle from X axis to the tangent of the riser at N_i;

Segment Angle θ_i is the angle from X axis to the line N_iN_{i+1};

Node Deflection Angle $\Delta\varphi_i$ is the angle between the tangents at N_i and N_{i+1};

Segment Deflection Angle $\Delta\theta_i$ is the angle from the tangent at N_i to the line N_iN_{i+1}.

According to the theories of Mechanics of Materials, the node deflection angle of the segment S_i is

$$\Delta\varphi_i = \frac{1}{EI}\int_0^{l_i}(m_i + \frac{m_{i+1} - m_i}{l_i}l)dl = \frac{(m_i + m_{i+1})}{2EI}l_i \tag{2}$$

where l_i is the length of S_i, E is Young's modulus, I is inertia moment of the cross-section area.

And the segment deflection angle of the segment S_i is

$$\begin{aligned}\Delta\theta_i &= \frac{1}{l_i}\int_0^{l_i}\frac{l}{2EI}\left[m_i+(m_i+\frac{m_{i+1}-m_i}{l_i}l)\right]dl \\ &= \frac{1}{2EIl_i}\left(\int_0^{l_i}2m_i l dl+\int_0^{l_i}\frac{m_{i+1}-m_i}{l_i}l^2 dl\right) \\ &= \frac{(2m_i+m_{i+1})}{6EI}l_i\end{aligned} \tag{3}$$

The node angle is

$$\varphi_{i+1}=\varphi_i+\Delta\varphi_i \tag{4}$$

The segment angle is

$$\theta_i=\varphi_i+\Delta\theta_i \tag{5}$$

where φ_1 is the node angle at N_1.

2.1.2 Displacements of Nodes

Since N_1 is the connection point of riser with the MV, the displacement of N_1 is determined by the motion of the MV.

For the node N_{i+1} (i=1, 2, …, n), the displacements is expressed by

$$\begin{cases}x_{i+1}=x_i+l_i\cos\theta_i\\ y_{i+1}=y_i+l_i\sin\theta_i\end{cases} \tag{6}$$

where (x_1, y_1) is the displacement of N_1, known beforehand.

For the riser in re-entry, the axial strain is ignored and l_i (i=1,2,…,n) is viewed as a constant. Consequently the velocity and acceleration of N_{i+1} are

$$\begin{cases}\dot{x}_{i+1}=\dot{x}_i-l_i\cdot\sin\theta_i\cdot\dot{\theta}_i\\ \dot{y}_{i+1}=\dot{y}_i+l_i\cdot\cos\theta_i\cdot\dot{\theta}_i\end{cases} \tag{7}$$

$$\begin{cases}\ddot{x}_{i+1}=\ddot{x}_i-l_i\cdot(\cos\theta_i\cdot\dot{\theta}_i^2+\sin\theta_i\cdot\ddot{\theta}_i)\\ \ddot{y}_{i+1}=\ddot{y}_i+l_i\cdot(-\sin\theta_i\cdot\dot{\theta}_i^2+\cos\theta_i\cdot\ddot{\theta}_i)\end{cases} \tag{8}$$

where $(\dot{x}_1, \dot{y}_1)$ and $(\ddot{x}_1, \ddot{y}_1)$ are the velocity and acceleration of N_1, known beforehand.

The displacement, velocity and acceleration vectors of N_i are denoted by

$$\begin{cases}\boldsymbol{r_i}=x_i\boldsymbol{i}+y_i\boldsymbol{j}\\ \dot{\boldsymbol{r}}_{\boldsymbol{i}}=\dot{x}_i\boldsymbol{i}+\dot{y}_i\boldsymbol{j}\\ \ddot{\boldsymbol{r}}_{\boldsymbol{i}}=\ddot{x}_i\boldsymbol{i}+\ddot{y}_i\boldsymbol{j}\end{cases} \tag{9}$$

2.2 Governing Equations

The governing equations are derived from the moment equilibrium at Nodes from

N_1 to N_n. The external forces exerted on the riser include: hydrodynamic force F_1, net buoyancy F_2 and inertia force F_3. In the non- inertial system of coordinates, these external forces must reach moment equilibrium at all nodes. The governing equations will be deduced according to moment equilibrium at nodes N_1 to N_n. Although other forces such as tension and shear forces also have effect on each segment, they are internal forces when concerning the whole riser, which shouldn't be included in the moment equilibrium. Thus, these internal forces are not discussed in this paper.

To simplify the calculation of external forces, we assume that the mass of and external forces on each segment are lumped at both end nodes averagely. The external forces acting on nodes can be calculated as follows.

2.2.1 External Forces on Nodes

Herein we adopt the semi-empirical Morrison approach for modeling hydrodynamics forces (Zhu Y. R, 1991; Pao H. P. et al, 2000). In this manner the fluid loads are decomposed into one component in phase with the fluid velocity (drag) and one component in phase with the fluid acceleration (added mass) (Howell C. T., 1992). The segment of riser can be viewed as a slightly oblique cylinder, and the hydrodynamic force can be decomposed into tangent, normal and bi- normal components. The tangent component is much smaller than the normal one, thus the hydrodynamic force of a segment of the riser is approximately equal to its normal component. Since the displacement caused by vortex-induced vibration is transverse and its influence is relatively small compared with the motion of riser, the effect of vortex-induced vibration is neglected in our two-dimensional analysis.

The hydrodynamic force on N_i (i=2, 3,…, n+1) can be calculated by

$$\boldsymbol{F}_{1,i} = \tfrac{1}{2} c_d \rho_w d_{o,i} l_{N,i} (\boldsymbol{v}_{wn,i} - \boldsymbol{v}_{n,i}) \left| \boldsymbol{v}_{wn,i} - \boldsymbol{v}_{n,i} \right| + c_M A_{o,i} l_{N,i} \rho_w \dot{\boldsymbol{v}}_{wn,i} - (c_M - 1) A_{o,i} l_{N,i} \rho_w \dot{\boldsymbol{v}}_{n,i} \quad (10)$$

where c_d, c_M are drag and inertia coefficients, $d_{o,i}$ is the outer diameter of riser at N_i, $A_{o,i}$ is the outer area of cross-section at N_i, ρ_w is water density, equal to 1025 kg/m^3; $l_{N,i}$ is the lumped length at N_i, $\boldsymbol{v}_{n,i}$ and $\dot{\boldsymbol{v}}_{n,i}$ are respectively the normal component of velocity vector $\boldsymbol{v}_i$ and the acceleration vector $\dot{\boldsymbol{v}}_i$ of N_i. The detailed calculation method of $l_{N,i}$, $\boldsymbol{v}_{n,i}$ and $\dot{\boldsymbol{v}}_{n,i}$ has been stated by Xu (2012). $\boldsymbol{v}_{wn,i}$ and $\dot{\boldsymbol{v}}_{wn,i}$ are the

normal component respectively of current velocity vector $\boldsymbol{v}_{w,i}$ and current acceleration vector $\dot{\boldsymbol{v}}_{w,i}$ at N_i.

Considering that cross-section areas at nodes are much smaller than the whole surface area of segment, the segment is viewed approximately as enclosed by water, and Archimede's principle can be applied. The net gravity on N_i is written as

$$\boldsymbol{F}_{2,i} = A_i l_{N,i} \rho_r \boldsymbol{g} \tag{11}$$

where A_i is the cross-section area of riser at N_i, $\boldsymbol{g}$ is the gravity vector, ρ_r is the riser average density in water.

According to D' Alembert's Principle, the inertia force at N_i is

$$\boldsymbol{F}_{3,i} = -A_i l_{N,i} \rho_r \ddot{\boldsymbol{r}}_i \tag{12}$$

By summing up the above $\boldsymbol{F}_{1,i}$, $\boldsymbol{F}_{2,i}$ and $\boldsymbol{F}_{3,i}$, the external forces acting on N_i (i = 2, 3, …, n+1) can be calculated:

$$\boldsymbol{F}_i = \boldsymbol{F}_{1,i} + \boldsymbol{F}_{2,i} + \boldsymbol{F}_{3,i} = F_{x,i}\boldsymbol{i} + F_{y,i}\boldsymbol{j} \tag{13}$$

For the riser with a bottom weight, the external force on N_{n+1} should include the bottom weight and its hydrodynamic force.

2.2.2 Moment Equilibrium

For each node N_i (i = 1, …, n), the external forces acting on nodes N_{i+1}, N_{i+2}, …, N_{n+1} must reach moment equilibrium:

$$m_i = \sum_{j=i+1}^{n+1} \left[-F_{x,j}(y_j - y_i) + F_{y,j}(x_j - x_i) \right] \tag{14}$$

where m_i is the bending moment of riser at N_i, and the right side of Equation (14) is the moment caused by external forces at nodes N_{i+1}, N_{i+2}, …, N_{n+1}.

According to moment equilibriums at N_1, N_2, …, N_n, n equations can be grouped. In the dynamic calculation, the moments at all nodes are variables to be solved, denoted by $\boldsymbol{m}$. Owing to the free connection of lower end, m_{n+1} equals to zero. So there are n variables and n equations.

2.3 Numerical Dynamic Calculation

In the dynamic calculation, the Finite Difference Method and the iteration method are applied. The interpolation equation is

$$\begin{cases} \dot{\boldsymbol{m}}(\Delta t) = \dfrac{\boldsymbol{m}(\Delta t) - \boldsymbol{m}(0)}{\Delta t} \\ \ddot{\boldsymbol{m}}(\Delta t) = \dfrac{\dot{\boldsymbol{m}}(\Delta t) - \dot{\boldsymbol{m}}(0)}{\Delta t} \end{cases} \tag{15}$$

where Δt is the time interval of iteration.

As for obtaining the numerical solution of the nonlinear equations, the MATLAB function “lsqnonlin” is employed.

3. Validation of Numerical Calculation

To validate the dynamic calculation, numerical results have been compared with experimental results.

Herein we adopt the experimental results of Hong (2004) for comparison. Experimental setup is shown in Fig.2. A hollow pipe made of Teflon and Polyethylene, together with a bottom weight, was used as the model in the experiment. The model upper end was fixed to the holding arm. The features of riser model are shown in Table 1.

Cameras were installed vertically to record the displacements of observation points A, B, …, E. The upper end of riser model oscillated sinusoidally along *X*-axis with the amplitude of 0.2m. The periods were 7s and 11s respectively. The riser model will respond with the same period also.

The experimental and numerical results of Hong are shown in Fig. 3-4 (a), solid lines represent the experimental results, while broken lines depict the numerical results. X_O is the displacement of upper end along *X* axis, while X_A, X_B, …, X_E are displacements along *X* axis at observation points A, B, …, E.

Numerical results obtained by the FSM based method are shown in Fig.3-4 (b). In the calculation, the riser model is divided into 20 segments, and the time interval of iteration is 0.01s, for the sake of the convergence of numerical calculation.

In the experiment, there is Vortex Induced Vibration (VIV). Its amplitude approximates 0.008m, much smaller than the riser oscillation amplitude, so VIV is neglected in the riser response. However, VIV will increase the drag coefficient c_d. According to the references of Koterayama’s experiments and Skop’s strumming

prediction, the drag coefficient c_d takes as 2.8, and inertia coefficient c_M generally takes the value of 2.0 in the our numerical calculation.

The steady-state responses of the observation points in the numerical calculation can be described by relative displacement to the upper end of the model in X direction. Graphs of experimental results provided by Hong (2004) and numerical results are put together in Fig.2-3 for the sake of comparison.

It can be seen from the comparison that the results of numerical calculation have fairly high accordance with the experiment results. That is to say, an accurate prediction of riser dynamic response can be obtained with the FSM, as long as suitable hydrodynamic coefficients have been applied.

4. Case Study

The dynamic response of a 1500m riser under horizontal oscillation of MV is analyzed in this section. The riser has the properties in Table 2. Its upper end is assumed fixedly connected with a mother vessel, which is subjected to horizontal oscillations with different amplitudes and periods. Its natural vibration periods are 9076s for the 1st order, 1448s for the 2nd order, and 517s for the 3rd order, according to the theory of Mechanical Vibrations (Rao, S. S., 2010).

When the riser oscillates in response to the horizontal oscillation of MV, a point that has the minimum oscillation amplitude along the whole riser exists. This point is named Minimum-Oscillation Point (MOP). In this section, the response of riser lower end is analyzed, and the MOP is located.

In the numerical calculation, the riser is divided into 20 segments during the iteration, and the values of time interval Δt are 0.01, 0.05, and 0.1 respectively for $T \le 10$, $10 < T < 50$, and $T \ge 50$, for the sake of the convergence of numerical calculation. Considering the vessel maneuverability, the horizontal oscillation period of mother vessel ranges from 0s to 2000s, although period of common wave-induced oscillations are much shorter than 2000s. The hydrodynamic coefficients c_M and c_d are equal to 2 and 1.2 respectively, as did by Xu (2012).

4.1 Response of Riser Lower End

Considering that the oscillation of riser lower end will cause difficulty during connection with the seabed wellhead, it is necessary to predict response of riser lower end under MV horizontal oscillations. The response amplitude of riser lower end under different MV oscillation amplitudes and periods is shown in Fig.5.

In Fig.5, the blue curve represents the response amplitude of riser lower end as the oscillation period changes in the case that MV horizontal oscillation amplitude $A_U = 5m$, while the purple curve and the yellow curve are for $A_U = 20m$ and $A_U = 35m$ respectively. It is noted that with the increase of the oscillation period T, the response amplitude of riser lower end (A_L) increases to a maximum response amplitude $A_{\max}$, and then declines. But the speed of descent is much slower than that of ascent. The maximum response amplitude and its corresponding oscillation period under different MV oscillation amplitudes are marked in the graph.

It can be seen that the oscillation periods when the maximum response amplitude occurs are 493.7s, 1226.7s, and 1730.0s respectively, corresponding to MV oscillation amplitudes of 5m, 20m, and 35m. One can further observe that $A_{\max}$ is larger than A_u. The increment is 18%, 4.5% and 2.6% respectively, corresponding to $A_U = 5m$, $A_U = 20m$ and $A_U = 35m$.

When comparing the curves of different oscillation amplitude, we can reach several conclusions:

(1) When the MV oscillation period T increases from 0s to 2000s, the general trend of response amplitude is to ascend first to $A_{\max}$, which is about 0.9m larger than the corresponding A_u, and then decline slightly. However, the relative increment of maximum response amplitude to the MV oscillation amplitude is larger when the MV oscillation amplitude is smaller.

(2)In spite of the gradual approach to the vessel oscillation amplitude in the declining stage after advent of $A_{\max}$, the response amplitude of riser lower end will not get smaller than A_u.

(3) If A_u rises, the oscillation period corresponding to $A_{\max}$ will also increase, and it's quite different from the natural vibration periods.

4.2 Minimum-Oscillation Point on Riser

As illustrated in Fig.6, the MOP on riser is marked in the case $A_U = 5m$ and $T = 200s$. Herein, the vertical coordinate denotes the distance from the upper end of the riser. The location of MOP is an important feature of the riser oscillation. It is hoped that the riser lower end could be MOP during re-entry, so that the difficulty of connection can be reduced. Therefore, we make dynamics calculation and analyze MOP along the riser.

Corresponding to different motion input of MV, the response amplitudes of all the 21 nodes are obtained in the dynamic calculation. Cubic spline interpolation is employed to plot the curve of response amplitude of different positions on the riser, and the point with minimum oscillation amplitude is picked out as MOP for each specific A_U and T. Fig.7 demonstrates the location of MOP at different oscillation amplitudes. Here the vertical coordinate is the distance from the riser upper end.

In Fig.7, the blue curve represents the response amplitude as T changes in the case of $A_U = 5m$, while the purple curve and the yellow curve are for $A_U = 20m$ and $A_U = 35m$ respectively. It is observed that when $A_U = 5m$ and $T > 500s$, MOP coincide with the riser upper end, while for $A_U = 20m$ and $A_U = 35m$ this coincidence occurs when $T > 1300s$ and $T > 1800s$ respectively.

On each curve, there is a strange phenomenon that the location of MOP fluctuates sharply when T is in the range of 0—30s. The fluctuant stages have been magnified and shown in Fig. 8, Fig. 9 and Fig. 10. At the beginning of the fluctuant stage in each case, the location of MOP on riser fluctuates rapidly. Afterwards, several flat stages will appear. Finally, the fluctuant stage will become relatively steady at around 1450m from the upper end of the riser. After going through the fluctuant stage, the ascent of MOP along the riser is inclined to become stable and regular before it reaches the upper end of the riser. The corresponding oscillation period T, at which the upper end of the riser coincides with MOP, tends to be longer if the A_U is larger.

Unstable as the graphs may seem, we can still reach several conclusions:

(1) The overall trend of the location of MOP is upward along the riser until it arrives at riser upper end, as T ascends.

(2) After the coincidence point at which riser upper end becomes the MOP, location

of MOP will not change henceforth, even if T continues to increase. That is to say, no matter what amplitude the mother vessel is oscillating at, if only T is large enough, no position on the riser will respond with a smaller amplitude than that of the MV.

(3) Instability exists when the T is shorter than 30s, after which MOP will go upward along the riser quickly as T goes up, until it reaches the smooth stage.

5. Sum-up

In this paper, we adopt the FSM based calculation method for analyzing the dynamic response of free hanging marine risers. Moment equilibrium equations are listed as governing equations, and the iteration method is employed to carry out numerical calculation. The comparison between experimental and numerical results is displayed, which validated the accuracy of the FSM based numerical calculation. Therefore, this method can be applied to the dynamic calculation of riser in re- entry.

In the dynamic calculation of a 1500m riser in re-entry, we analyze the dynamic response of riser lower end, and locate the MOP on the riser, as A_U and T change. With regard to the response of riser lower end, as T increases, the general trend is upward till $A_{\max}$ occurs, and then A_L declines slightly, approaching A_U . Another conclusion is that the T corresponding to $A_{\max}$ tends to increase when A_U rises. When it comes to MOP, the overall trend of its location is upward along the riser as T increases, until it is located at the riser upper end, and then remains invariable. Nevertheless, the location of MOP fluctuates sharply when T is below 30s in our case study. To conclude, taking the location of MOP and A_L into consideration, A_U and T should both be kept small in order to carry out a successful and cost effective installation.

However, limitations still exist in our study and further research is still in need. The influence of wave and current hasn't been taken into consideration, and the analysis of riser response is still confined to 2-dimensional. In the future, we will continue the study about the FSM based dynamics calculation: (1) Influence of wave and current on the response of marine riser will be probed into. (2) Motion of mother vessel in multiple directions, such as in heaving and swaying, and so on, will also be taken into consideration, and the analysis of riser response will be extended to these complex

cases.

References

Bai, X. L., Huang, W. P., Varz, M. A., Yang, C. F. and Duan, M. L., 2015. Riser-soil interaction model effects on the dynamic behavior of a steel catenary riser, *Marine Structures*, **41**(4):53~75.

Chen, W. M., Li, M., Guo, S. X. and Gan, K., 2014. Dynamic analysis of coupling between floating top-end heave and riser's vortex-induced vibration by using finite element simulations, *Applied Ocean Research,* **48**(10):1~9

Dai, H. L., Abdelkefi, A. and Wang, L., 2014. Modeling and nonlinear dynamics of fluid-conveying risers under hybrid excitations, *International Journal of Engng. Science,* **81**(8): 1~14.

Do, K. D. and Pan, J., 2008. Reducing transverse motion of marine risers with actuator dynamics by boundary control, *Proc. of 10th International Conference on Control, Automation, Robotics and Vision*, Hanoi, Vietnam, 307~312.

Do, K. D. and Pan, J., 2008. Boundary control of transverse motion of marine risers with actuator dynamics, *Sound and Vibration*, **318** (4-5): 768~791.

Hong, Y. P., 2004. *A Study on dynamics of flexible marine riser,* Ph. D thesis, Kyushu University.

Hosseini Kordkheili, S. A., Bahai, H. and Mirtaheri, M., 2011. An updated Lagrangian finite element formulation for large displacement dynamic analysis of three-dimensional flexible riser structures, *Ocean Engng.*, **38** (5-6): 793~803

Howell, C. T., 1992. *Investigation of the Dynamics of Low-tension cables,* Ph. D thesis, Massachusetts Institute of Technology.

Kajiwara, H. and Noridomi, K., 2009. Reentry control system design for a riser pipe experimental model under steady current, *Proc. of International Joint Conference*, Fukuoka, Japan, 3896~3901.

Koterayama W., Nakamura M., 1988. Wave forces acting on a moving cylinder. *Journal of Offshore Mechanics and Arctic Engineering*, 110, 315-319.

Lucor, D. and Triantafyllou, M. S., 2008. Riser response analysis by modal phase reconstruction, *Offshore Mechanics and Arctic Engineering*, **130**(1): 011008～011016.

Pao, H.P., Ling, S. C. and Kao, T. W., 2000. Measurement of axial hydrodynamic force on a yawed cylinder in a uniform stream, *Proc. of the 10th Offshore and Polar Engng. Conference*, Seattle, USA, 356~361.

Park, H. I. and Jung, D. H., 2002. A finite element method for dynamic analysis of long slender marine structures under combined parametric and forcing excitations, *Ocean Engng.*, **29**(11): 1313~1325.

Park, H. I. and Jung, D. H., 2003. A numerical and experimental study on dynamics of a towed low tension cable, *Applied Ocean Research*, **25**(5): 289~299.

Patel, M. H. and Seyed, F. B., 1995. Review of flexible riser modeling and analysis techniques, *Engng. Structures*, **17**(4): 293~304.

Quéau, L. M., Kimiaei, M. and Randolph, M. F., 2013. Dimensionless groups governing response of steel catenary risers, *Ocean Engng.*, **74**(12): 247~259.

Ramam-nair, W. and Baddour, R. E., 2003. Three-dimensional dynamics of a flexible marine riser undergoing large elastic deformations, *Multibody system dynamics*, **10**(4): 393~423.

Rao, S. S., 2010. *Mechanical Vibrations*. Prentice Hall Press, P721-739.

Skop R.A., Griffin O.M., Ramberg S.E., 1977. Strumming predictions for the SEACON II experimental mooring. *Offshore Technology Conference*, Houston, 61-66.

Srinil, N., 2011. Analysis and prediction of vortex-induced vibrations of variable-tension vertical risers in linearly sheared currents, *Applied Ocean Research*, **33**(2): 41~53.

Wang, J. G., Fu, S. X., Baarholm, R., Wu, J. and Larsen, C. M., 2014. Fatigue damage of a steel catenary riser from vortex-induced vibration caused by vessel motions, *Marine Structures*, **39**(12): 131~156.

Xiao, F. and Yang, H. Z., 2014. Instability analyses of a top-tensioned riser under combined vortex and multi-frequency parametric excitations, *Ocean Engng.*, **81**(5):12~28.

Xu, E., Koterayama, W. and Nakamura, M., 2007. A development of image analysis scheme for the control of the riser end, *Proc. of the 17th International Offshore and Polar Engng. Conference*, Lisbon, Portugal, 871~878.

Xu, J., He, M. and Bose, N., 2009. Vortex modes and vortex-induced vibration of a long flexible riser, *Ocean Engng.*, **36**(6-7): 456~467.

Xu, X. and Wang, S., 2012. A flexible-segment-model-based dynamic calculation method for free hanging marine risers in re-entry, *China Ocean Engng.*, **26**(1):139~152

Xu, X. S., Yao, B. H. and Ren, P., 2013. Dynamics calculation for underwater moving slender bodies based on flexible segment model, *Ocean Engng.*, **57**(1):111~127

Yang, M., Teng, B., Ning, D. and Shi, Z., 2012. Coupled dynamic analysis for wave interaction with a truss spar and its mooring line/riser system in time domain, *Ocean Engng.*, **39**(1): 72~87.

Zhu, Y. R., 1991. *Wave mechanics for ocean engineering*, Tianjin University Press, 69~94.

Nomenclature

S_i — The i^{th} flexible segment

N_i — The i^{th} node of the flexible segments

m_i — Bending moment at N_i , N•m

l_i — Length of segment S_i, m

φ_i — Node angle from X-axis to the tangent of the riser at N_i, rad

θ_i — Segment angle from X-axis to the line N_iN_{i+1}, rad

$\Delta\varphi_i$ — Node deflection angle between the tangents at N_i and N_{i+1}, rad

$\Delta\theta_i$ — Segment deflection angle from the tangent at N_i to the line N_iN_{i+1}, rad

x_i — Displacement along X-axis at N_i, m

y_i — Displacement along Y-axis at N_i, m

$l_{N,i}$ — Lumped length at N_i, m

A_i — Cross-section area of riser at N_i, m^2

$\boldsymbol{g}$ — Gravity vector, m^2/s

ρ_r — Riser average density in water, kg/m^3

$\boldsymbol{F}_{1,i}$ — Hydrodynamic force on N_i, N

$\boldsymbol{F}_{2,i}$ — Net gravity on N_i, N

$\boldsymbol{F}_{3,i}$ — Inertia force at N_i, N

$\boldsymbol{F}_i$ — External force acting on N_i , N

Δt — Time interval of iteration, s

T — Period of horizontal oscillation of mother vessel, s

A_U — Amplitude of horizontal oscillation of riser upper end, m

A_L — Amplitude of response of riser lower end, m

Table Captions

Tab. 1. Features of the Riser Model in Hong's Experiment

Tab. 2. Properties of the 1500-meter Riser

Table 1 Properties of the riser model in Hong's experiment

Length	Outer Diameter	Inner Diameter	Density in Water	Density in Air	Young's Modulus	Bottom Weight (Diameter× Length)
6.5 m	0.0225 m	0.0127 m	476.4 kg/m^3	1476.4 kg/m^3	3.487× 10^{6}Pa	3.489 N (0.032 m× 0.060 m)

Table 2 Properties of the 1500m Riser

Length	Outer Diameter	Inner Diameter	Density in Water	Density in Air	Young's Modulus
1500 m	0.4064 m	0.3747 m	2100 kg/m^3	3095 kg/m^3	2.07× 10^{11}Pa

Figure Captions

Fig.1. Flexible segment model.

Fig.2. Experimental setup. Cameras are used to observe displacements of observation points A, B, …, E.

Fig.3. Displacement time history of the model as the upper end oscillates at the period of 7s: (a) experimental results (solid lines) provided by Hong. X_0, X_A, X_B, ..., X_E are displacements of model upper end and observation points A, B, ..., E; (b) numerical results by FSM based optimization method.

Fig.4. Displacement time history of the model as the upper end oscillates at the period of 11s: (a) experimental results (solid lines) provided by Hong. X_0, X_A, X_B, ..., X_E are displacements of model upper end and observation points A, B, ..., E; (b) numerical results by FSM based optimization method.

Fig.5. Response amplitude of riser lower end with the change of horizontal oscillation period T. The horizontal oscillation amplitudes of mother vessel $A_U = 5m$, $A_U = 20m$, and $A_U = 35m$ respectively. $A_{\max}$ is the maximum response amplitude of riser lower end.

Fig.6. Riser shapes under $A_U = 5m$ and $T = 200s$. $P_{\min}$ is the minimum- oscillation point (MOP) on riser

Fig.7. Location of MOP on riser along with the variance of T when the oscillating amplitude of mother vessel $A_U = 5m$, $A_U = 20m$, and $A_U = 35m$ respectively

Fig.8. Amplification of the fluctuant stage in the graph of distance from riser upper end of MOP along with the variance of T when $A_U = 5m$

Fig.9. Amplification of the fluctuant stage in the graph of distance from riser upper end of MOP along with the variance of T when $A_U = 20m$

Fig.10. Amplification of the fluctuant stage in the graph of distance from riser upper end of MOP along with the variance of T when $A_U = 35m$

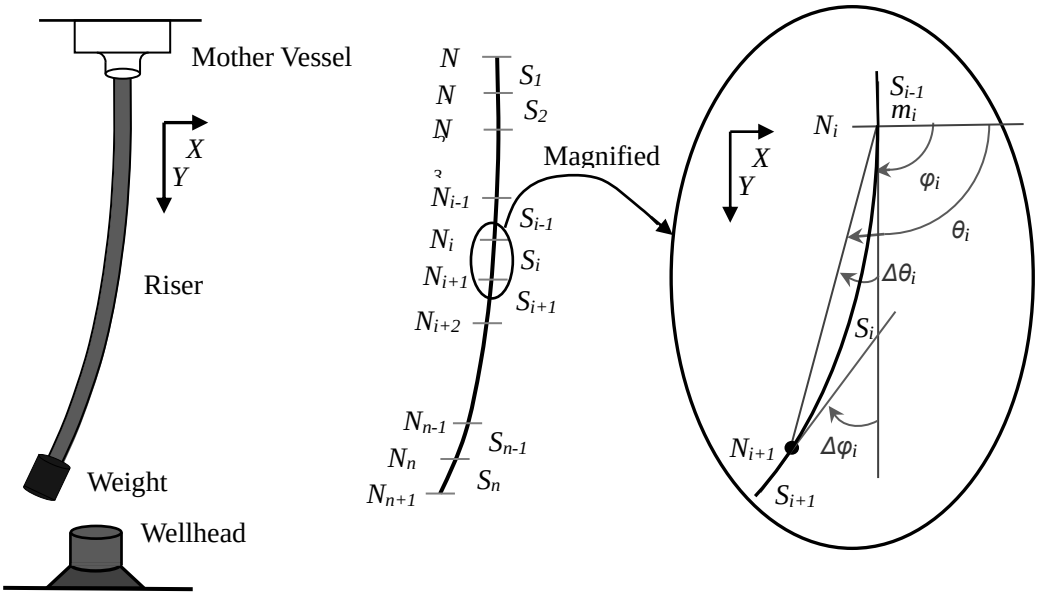

(a) Riser in re-entry (b) Riser discretization (c) Magnification of segment S_i

Fig.1. Flexible segment model.

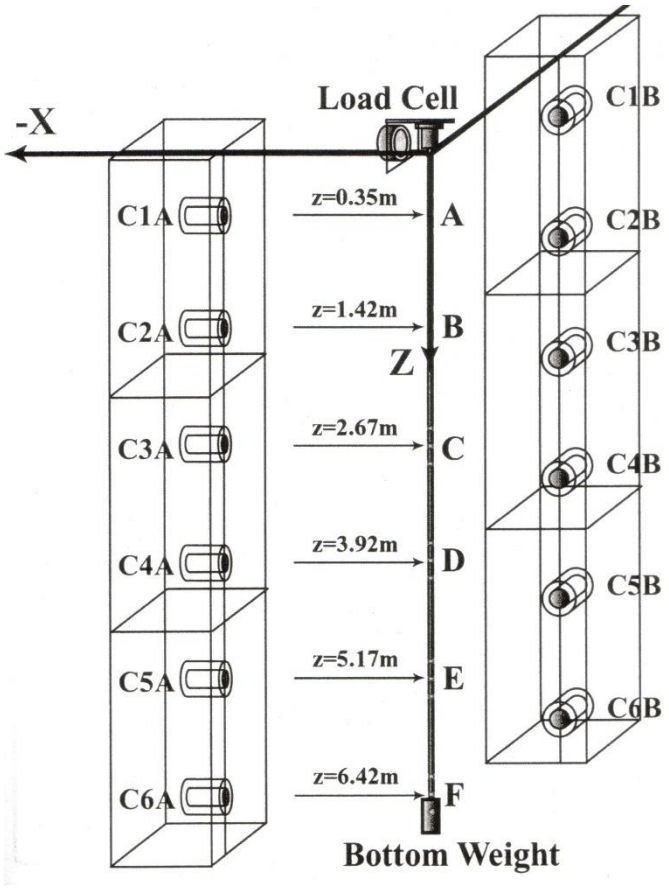

Fig. 2. Experimental setup. Cameras are used to observe displacements of observation points A, B, …, E.

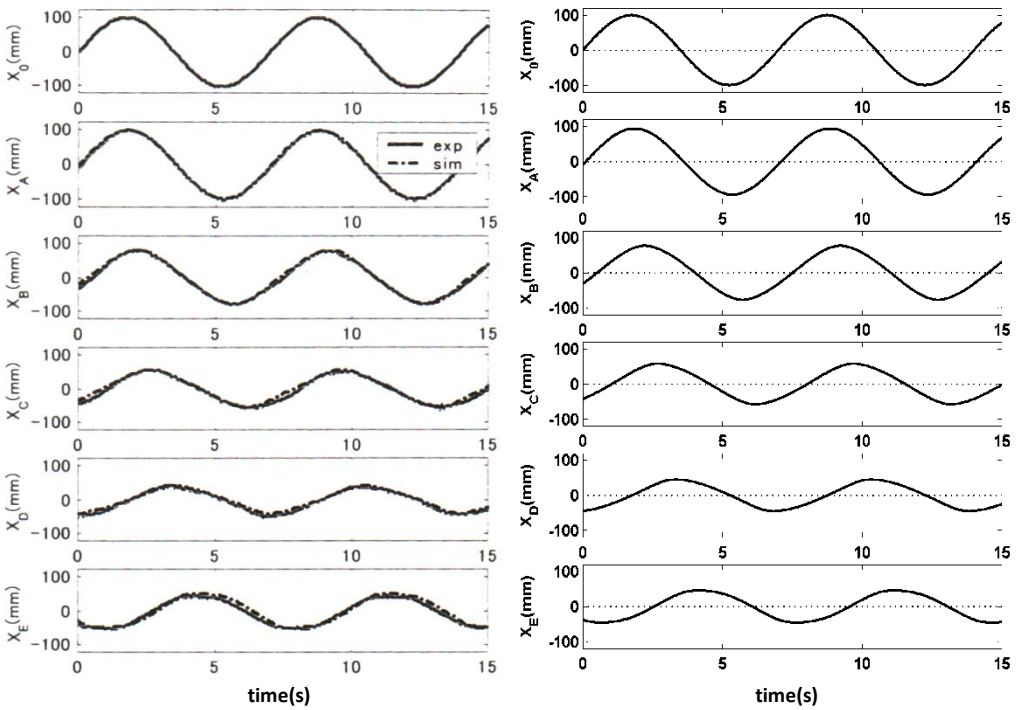

(a) (b)

Fig.3. Displacement time history of the model as the upper end oscillates at the period of 7s: (a) experimental results (solid lines) provided by Hong. X_0, X_A, X_B, ..., X_E are displacements of model upper end and observation points A, B, ..., E; (b) numerical results by FSM based optimization method.

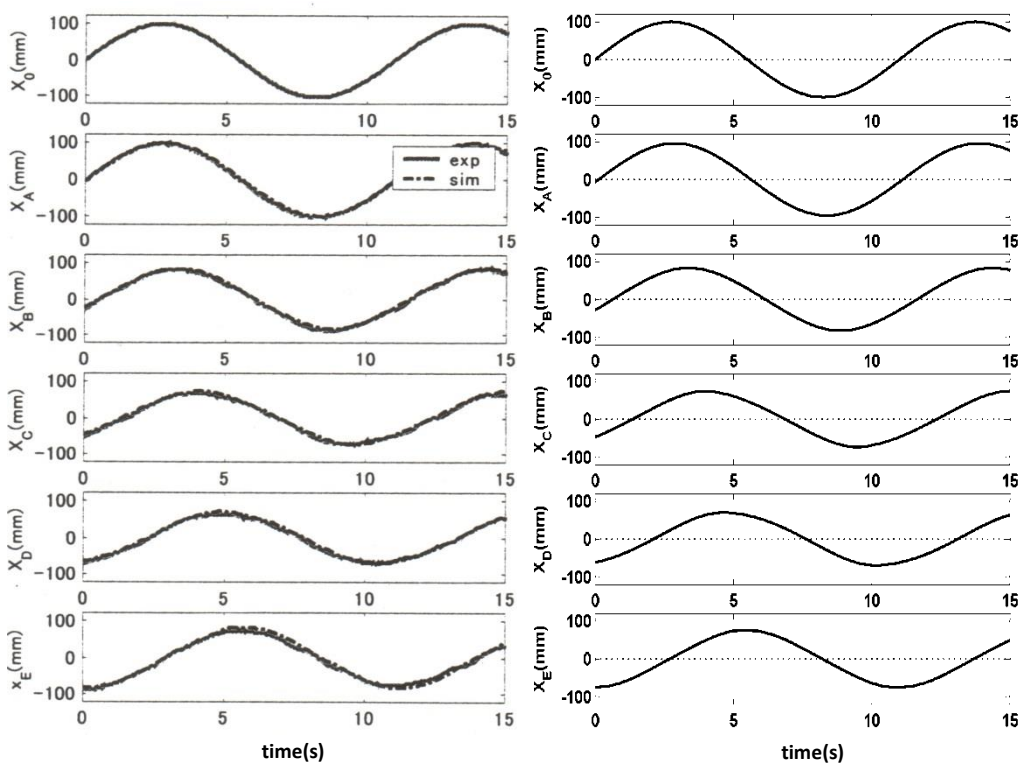

(a) (b)

Fig.4. Displacement time history of the model as the upper end oscillates at the period of 11s: (a) experimental results (solid lines) provided by Hong. X_0, X_A, X_B, ..., X_E are displacements of model upper end and observation points A, B, ..., E; (b) numerical results by FSM based optimization method.

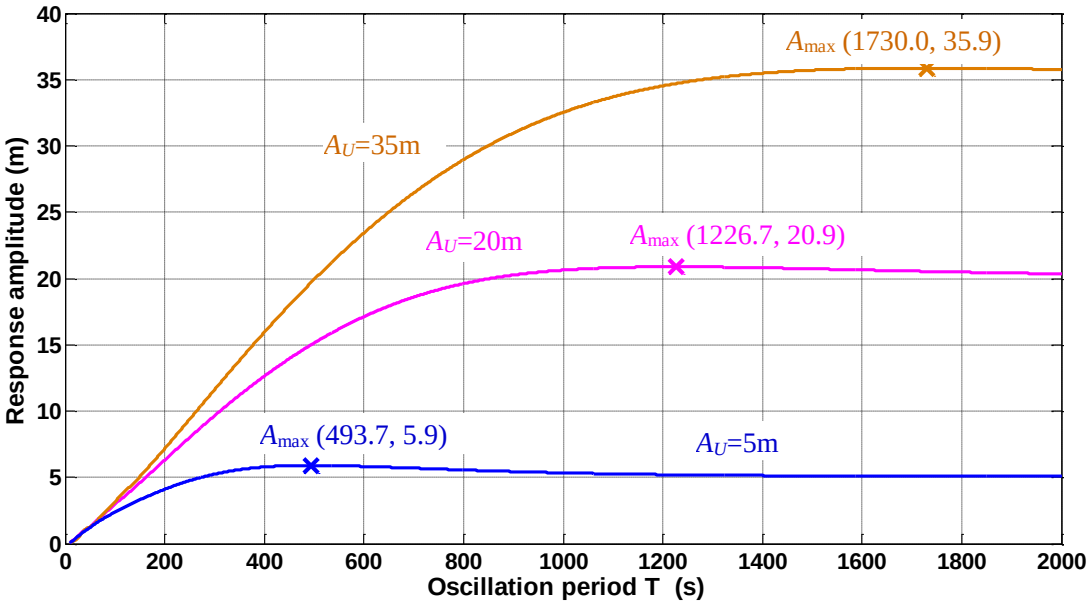

Fig. 5. Response amplitude of riser lower end with the change of horizontal oscillation period T. The horizontal oscillation amplitudes of mother vessel $A_U = 5m$, $A_U = 20m$, and $A_U = 35m$ respectively. $A_{\max}$ is the maximum response amplitude of riser lower end.

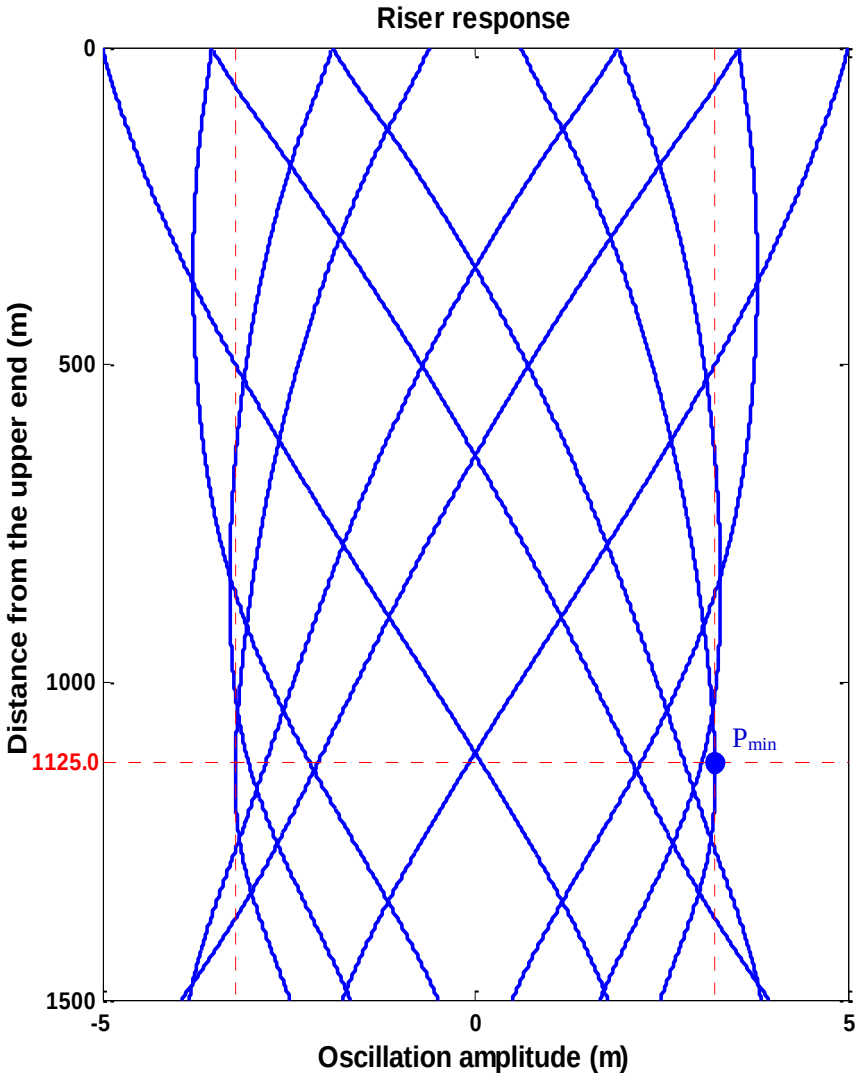

Fig.6. Riser shapes under $A_U = 5m$ and $T = 200s$. $P_{\min}$ is the minimum- oscillation point (MOP) on riser.

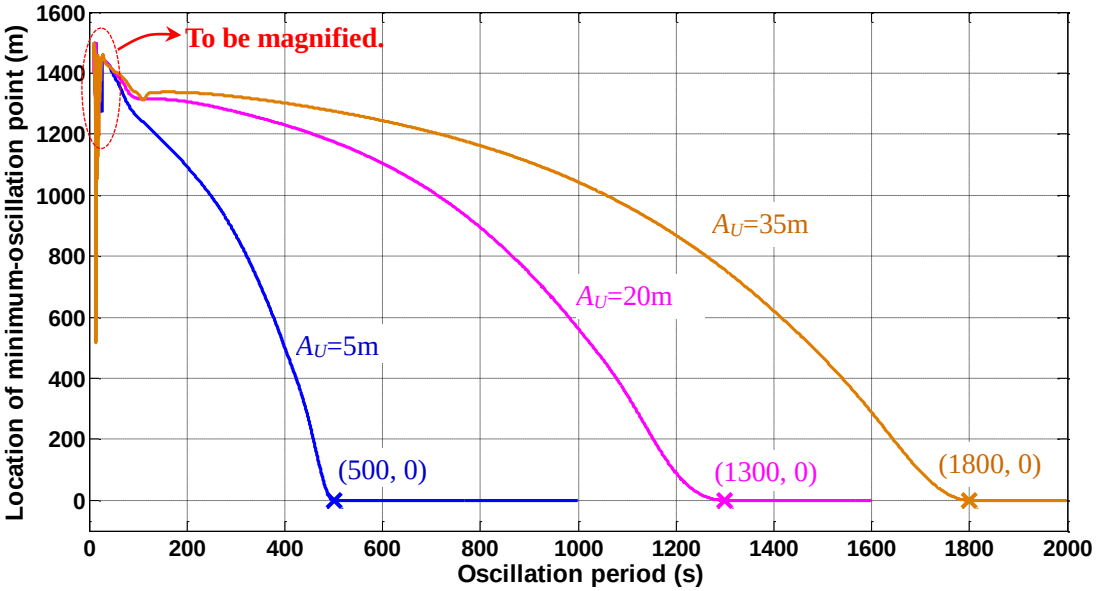

Fig.7. Location of MOP on riser along with the variance of T when the oscillating amplitude of mother vessel $A_U = 5m$, $A_U = 20m$, and $A_U = 35m$ respectively

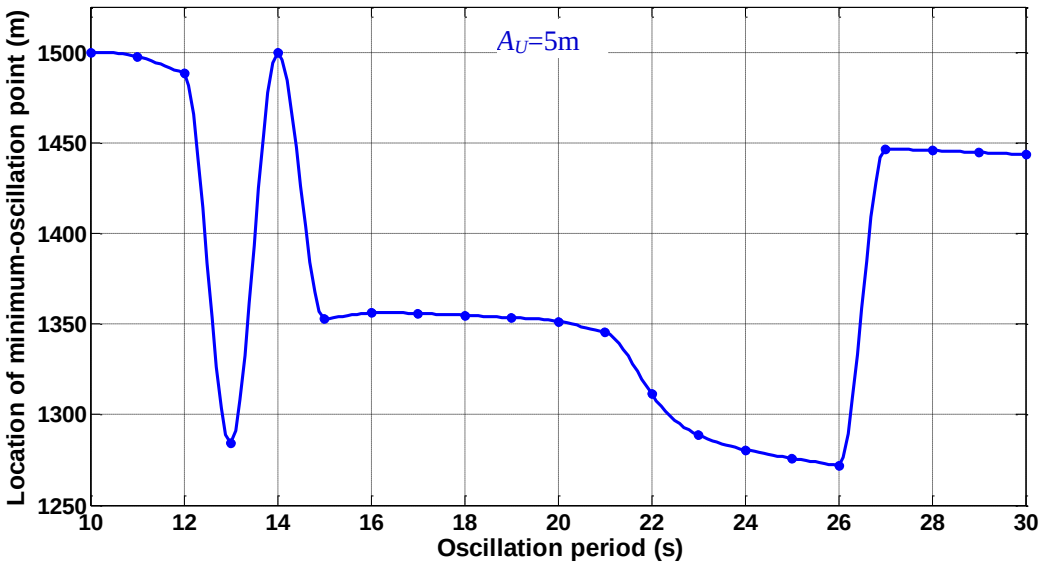

Fig.8. Magnification of the fluctuant stage in the graph of distance from riser upper end of MOP along with the variance of T when $A_U = 5m$

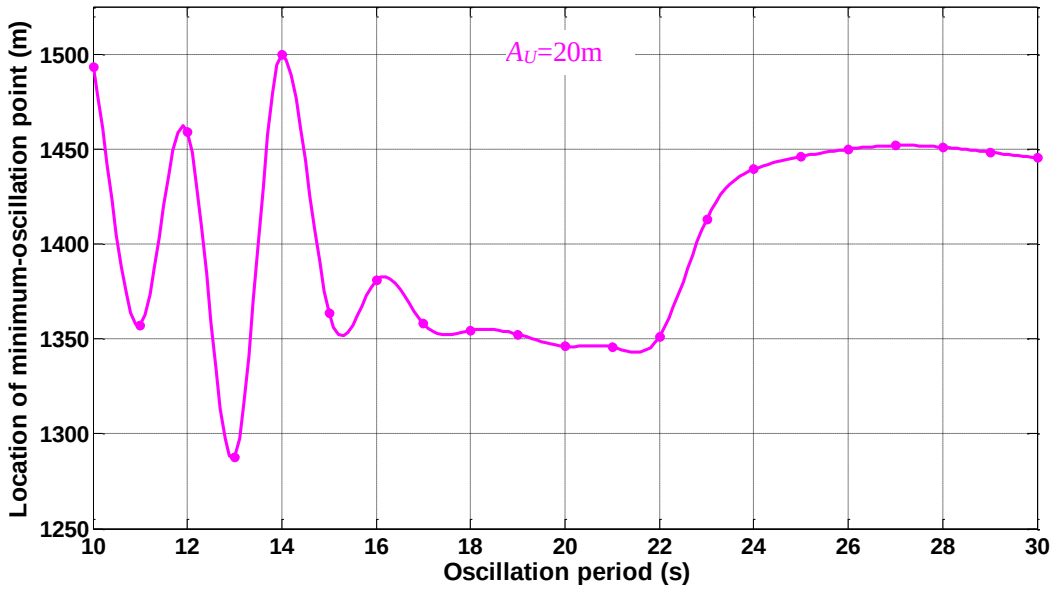

Fig.9. Magnification of the fluctuant stage in the graph of distance from riser upper end of MOP along with the variance of T when $A_U = 20m$

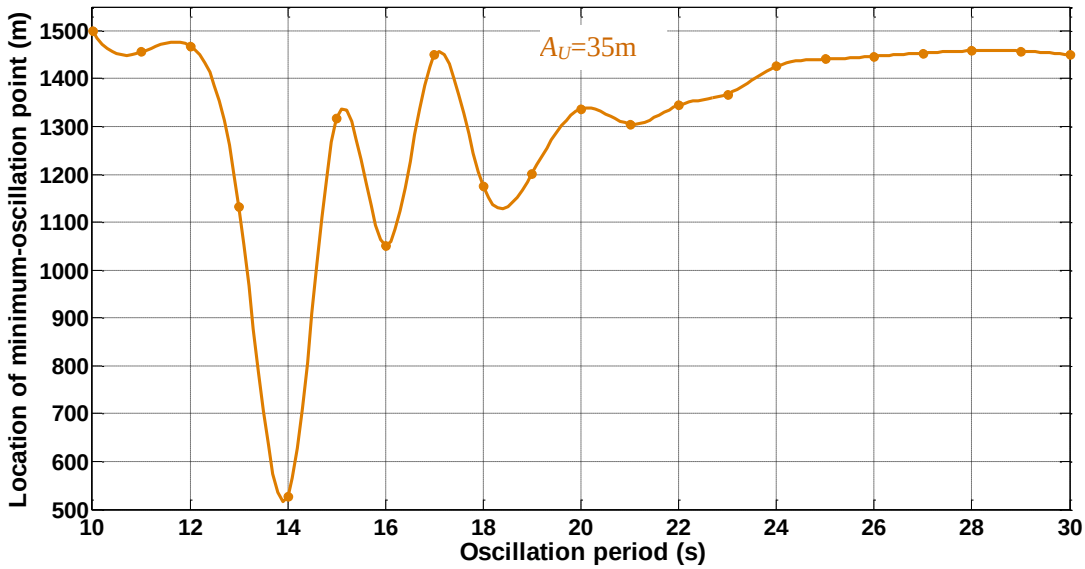

Fig.10. Magnification of the fluctuant stage in the graph of distance from riser upper end of MOP along with the variance of T when $A_U = 35m$